Check for updates

Journal of Pineal Research

WILEY

Journal of Pineal Research
Molecular, Biological, Physiological and Clinical Aspects of Melatonin

ORIGINAL ARTICLE OPEN ACCESS

Light-Dependent Circadian Rhythm Governs *O*-GlcNAc Cycling to Influence Cognitive Function in Adult Zebrafish

Jiwon Park[1] | Dong Yeol Kim[1] | Eok-Soo Oh[2] | Inn-Oc Han[1]

[1]Department of Biomedical Science, Program in Biomedical Science and Engineering, Department of Physiology and Biophysics, College of Medicine, Inha University, Incheon, Korea | [2]Department of Life Sciences, Ewha Womans University, Seoul, Korea

Correspondence: Inn-Oc Han (iohan@inha.ac.kr)

Received: 17 May 2024 | **Revised:** 18 July 2024 | **Accepted:** 23 July 2024

Funding: This work was supported by National Research Foundation (NRF) of Korea Grants (RS-2024-00346770) and Research Grant of Inha University.

Keywords: circadian cycle | hexosamine biosynthetic pathway | histone modification | zebrafish

ABSTRACT

This study explores the 24-h rhythmic cycle of protein *O*-GlcNAcylation within the brain and highlights its crucial role in regulating the circadian cycle and neuronal function based on zebrafish as an animal model. In our experiments, disruption of the circadian rhythm, achieved through inversion of the light-dark cycle or daytime melatonin treatment, not only impaired the rhythmic changes of *O*-GlcNAcylation along with altering expression patterns of *O*-GlcNAc transferase (OGT) and *O*-GlcNAcase (OGA) in zebrafish brain but also significantly impeded learning and memory function. In particular, circadian disruption affected rhythmic expression of protein *O*-GlcNAcylation and OGT in the nuclear fraction. Notably, the circadian cycle induces rhythmic alterations in *O*-GlcNAcylation of H2B histone protein that correspond to changes in H3 trimethylation. Disruption of the cycle interfered with these periodic histone code alterations. Pharmacological inhibition of OGT with OSMI-1 disrupted the wake-sleep patterns of zebrafish without affecting expression of circadian rhythm-regulating genes. OSMI-1 inhibited the expression of *c-fos*, *bdnf*, and *calm1*, key genes associated with brain function and synaptic plasticity, and decreased the binding of *O*-GlcNAcylated H2B and OGT to promoter regions of these genes. The collective findings support the potential involvement of circadian cycling of the *O*-GlcNAc histone code in regulating synaptic plasticity and brain function. Overall, data from this study provide evidence that protein *O*-GlcNAcylation serves as a pivotal posttranslational mechanism integrating circadian signals and neuronal function to regulate rhythmic physiology.

1 | Introduction

Circadian clocks are innate to organisms across all domains of life, governing endogenous oscillations with a duration of approximately 24 h that synchronize with environmental cues, such as light, temperature, and food [1]. These internal timers perceive daily environmental rhythms and regulate the timing of physiological and metabolic processes to optimize energy homeostasis [2]. Light serves as a primary signal for entraining endogenous circadian clocks with the light-dark cycle, regulating the central clock of the organism. In mammals, light information is relayed from the retina to the suprachiasmatic nuclei (SCN) in hypothalamus, which serves as the master clock. However, zebrafish possess a unique ability to directly detect light through photoreceptors in the pineal gland, which produces melatonin in response to the onset of darkness and thereby plays a central role in regulating circadian rhythms [3, 4].

Jiwon Park and Dong Yeol Kim contributed equally to this study.

This is an open access article under the terms of the Creative Commons Attribution-NonCommercial-NoDerivs License, which permits use and distribution in any medium, provided the original work is properly cited, the use is non-commercial and no modifications or adaptations are made.

© 2024 The Author(s). *Journal of Pineal Research* published by John Wiley & Sons Ltd.

The oscillation of circadian-regulated genes is regulated by a molecular clock feedback loop, which operates throughout the light-dark cycle in both mammals and zebrafish [3, 5]. The BMAL1/CLOCK heterodimer has been shown to drive expression of period (*Per1*, *Per2*, and *Per3*) and cryptochrome (*Cry1* and *Cry2*) genes. The resulting PER and CRY proteins inhibit their own transcription by impeding BMAL1/CLOCK activity. Rhythmic expression of the nuclear receptor NR1D1 (REV-ERB) is additionally controlled by BMAL1/CLOCK, and conversely, NR1D1 inhibits BMAL1 expression. Another well-known circadian regulation cue is the feeding-fasting cycle, which primarily controls peripheral clocks in organs, such as the liver, muscles, lungs, and heart [6]. Synchronization of the external environmental cues with the internal circadian rhythm is essential for maintaining organismal homeostasis and discordance between these two clocks that triggers circadian rhythm disruption. In humans, factors such as artificial light exposure at night, insufficient sunlight exposure during the day, shift work, brain damage (e.g., stroke and dementia), aging, and jet lag contribute to circadian disruption, which is associated with a range of metabolic, tumoral, and neurological disorders [7–10]. To ascertain the physiological importance and underlying mechanisms of circadian rhythm and identify therapeutic targets for circadian disorders, numerous studies have employed circadian disruption models induced by disrupting the light-dark cycle, restricting food consumption time, and manipulating melatonin or circadian rhythm-regulating genes [11–13]. Light-dark shifting, in particular, a relatively noninvasive method for modeling circadian disruption, has been widely used [14–16].

The circadian clock has emerged as a fundamental mechanism that governs metabolism [17], orchestrating the daily rhythmic expression of genes involved in glucose and lipid metabolism [17, 18]. While significant strides have been made in understanding the coordination between the circadian clock and metabolism in modulating circadian physiology, the central regulatory mechanisms remain largely unknown. The hexosamine biosynthetic pathway (HBP) of glucose metabolism has been identified as a potential coordinated mediator of circadian regulation. HBP serves as a generalized sensor for metabolic status, integrating metabolites generated from the breakdown of glucose, amino acids, lipids, and nucleic acids [19]. The end-product, uridine diphosphate-*N*-acetylglucosamine (UDP-GlcNAc), produced by HBP serves as a substrate for *O*-GlcNAcylation at serine and threonine residues of target proteins. *O*-GlcNAcylation is dynamically regulated by *O*-GlcNAc transferase (OGT) and *O*-GlcNAcase (OGA) that are responsible for the addition and removal of *O*-GlcNAc, respectively. Multiple studies have shown that circadian clocks drive daily fluctuations in protein *O*-GlcNAcylation [20–22]. Furthermore, gene expression profiles indicate circadian rhythms in *Gfat-1, Ogt,* and *Oga* transcripts in metabolic tissues [23]. Notably, circadian changes in *O*-GlcNAcylation of clock proteins, such as BMAL1, CLOCK, and PER, have been reported [20–22]. However, it is not clear whether cellular proteins derived from various metabolic genes beyond the circadian oscillator also exhibit daily *O*-GlcNAcylation rhythms. Furthermore, the regulatory mechanisms and potential functional roles of daily *O*-GlcNAc cycling in the circadian cycle are yet to be elucidated. The consequences of disruption of *O*-GlcNAc cycling in the brain on the circadian cycle and brain function also remain to be established.

Histone proteins undergo various posttranslational modifications, including acetylation, methylation, phosphorylation, ubiquitination, and *O*-GlcNAcylation [24], which alter the structure of histone-DNA complexes and affect gene expression levels [25]. Histone 3 lysine 4 tri-methylation (H3K4me3) and histone 3 lysine 9 acetylation (H3K9ac) are among the most common modifications associated with active chromatin markers while histone 3 lysine 9 methylation (H3K9me) is considered a repressive marker [26]. Additionally, OGT-induced *O*-GlcNAcylation of the H2B tail at Ser112 has been reported, with levels fluctuating in response to extracellular glucose through the HBP, in turn, promoting monoubiquitination of H2B at K120 and transcriptional activation [27, 28]. OGT not only directly catalyzes *O*-GlcNAcylation but is also involved in other histone modifications by indirectly catalyzing other modifier enzymes [29]. The enzyme forms complexes with ten-eleven translocation (TET) proteins that induce histone demethylation, generating H3K4me3 [30]. However, the roles, implications, and underlying regulatory mechanisms of H2B *O*-GlcNAcylation remain largely unexplored. In particular, comprehensive investigation of the potential role of histone *O*-GlcNAcylation in regulation of the circadian cycle or maintaining normal brain function should be a focus of further research.

Zebrafish have emerged as an excellent and useful model system for sleep and behavioral research [31]. Zebrafish are diurnal species that sleep at night or in hours of darkness like humans, in contrast to nocturnal species, such as mice, that sleep during the day [32]. Zebrafish possess clock-driven genes that regulate the sleep and arousal cycle following the light-dark phase. In this study, we employed two circadian disruption models of adult zebrafish: (1) circadian disruption induced by light-dark cycle inversion and (2) circadian disruption induced by melatonin treatment at the onset of the light phase. Data acquired from these models confirmed the impairment of daily circadian rhythm and concomitant disruption of *O*-GlcNAcylation and OGT expression that contributed to abnormal brain function. In the current study, we investigated the complex interplay among circadian rhythms, metabolism, epigenetics, and brain function, with particular focus on the impacts of circadian disruption on *O*-GlcNAc cycling and normal brain function in adult zebrafish.

2 | Materials and Methods

2.1 | Chemicals and Reagents

Chemicals and reagents were procured from Sigma Aldrich (St. Louis, MO) or Tocris (Bristol, UK), unless otherwise specified.

2.2 | Cell Culture

The mouse neuroblastoma cell line, N2A cells [33], was cultured in Dulbecco's Modified Eagle's Media (DMEM, Hyclone, Chicago, IL) supplemented with 5% fetal bovine serum (FBS, GE Healthcare, Chicago, IL) and 1× penicillin/streptomycin (HyClone). Cells were maintained at 37°C with

16000736, 2024, 5, Downloaded from https://onlinelibrary.wiley.com/doi/10.1111/jpi.13001 by Ewha Womans University Library, Wiley Online Library on [10/11/2024]. See the Terms and Conditions (https://onlinelibrary.wiley.com/terms-and-conditions) on Wiley Online Library for rules of use; OA articles are governed by the applicable Creative Commons License

5% CO_2. To confirm the effect of melatonin, cells were treated with melatonin or 1% EtOH at indicated concentrations and times. For circadian rhythm synchronization, cells were treated for 90 min with 200 nM dexamethasone in DMEM with 0.25% FBS. Subsequently, the media was replaced with fresh DMEM containing 0.25% FBS with OSMI-1 (50 μM) or 0.1% DMSO [34, 35].

2.3 | Zebrafish Handling

All zebrafish-based procedures used in this study complied with ethical guidelines and protocols approved by the Institutional Animal Care and Use Committee of Inha University (Approval No: INHA 220719-832, Incheon, Korea). Adult zebrafish (*Danio rerio,* AB strain) aged 3–6 months were procured from Fishzzang (Jinchun, Korea) and maintained under standard conditions at a temperature of 26 ± 1°C in housing water filtered and supplemented using a multistage filtration system comprising sediment, pre-carbon, membrane, and post-carbon filters. Fish tanks were equipped with apparatus that allowed continuous aeration, and pH levels were consistently maintained between 6.5 and 7.5. Lights were automatically turned on for 12 h from 8 a.m. to 8 p.m. The circadian disruption group was exposed to a reverse light cycle, with illumination from 8 p.m. until 8 a.m. the next day. This reversal was initiated over a 3-day period following a minimum of 2 weeks of exposure to the standard control light cycle to establish a stable baseline. To minimize potential circadian rhythm influences due to feeding, zebrafish were provided with flake food (TetraBits, Luzerne, Singapore) daily during transitions between the light/dark phases. All experiments and measurements were conducted in a blinded and randomized manner and included both male and female zebrafish (~50:50 male:female ratio).

2.4 | Drug Injection

In terms of drug administration, specific groups of zebrafish received an intraperitoneal injection of either melatonin (50 μg/g) or 0.1% EtOH using a Hamilton syringe (Hamilton, NV, USA) at 8 a.m. or 8 p.m. for three consecutive days. Another set of groups received OSMI-1 (0.01 ng/g) or 0.1% DMSO that was injected into the skull of zebrafish using the same syringe at 8 p.m. for three consecutive days. Subsequently, zebrafish were returned to their home tanks, and any injection errors were identified and excluded based on observed changes in swimming patterns.

2.5 | Fear Context Learning and Memory Test

To assess learning and memory (L/M) ability, contextual fear conditioning (FC) tests were conducted following previously described methods [36]. At least 1 h before the test, zebrafish were acclimated in the testing room under normal housing conditions, and tests were conducted between 9 a.m. and 7 p.m. The FC tank was constructed from black acrylic with dimensions of 18.5 cm in length, 7 cm in width, and 10 cm in depth (Supporting Information S1: Figure 1). It consisted of two compartments: a dark room and a light room. These rooms were separated by a partition with a 3 cm diameter hole. At the beginning of the test, each zebrafish was placed in a dark room of the testing chamber to stabilize for 3 min. During the fish stabilization time, the hole in the partition was blocked by a sliding door. Following stabilization, the sliding door was opened to allow the fish to move into the light room. Upon crossing into the light room, the time taken to cross was recorded, followed by inducing fear in the fish by tapping the front of the zebrafish with a stone. The crossing time was measured for up to 5 min in each trial. The fish were then transferred back to the dark room, and this process was repeated two more times. For the memory test, the crossing time was measured similarly to the FC training but without inducing fear. The memory test was conducted 2 h after the training session.

2.6 | Actogram Measurement

To assess sleep and activity patterns in adult zebrafish, actogram measurements were conducted using an infrared sensor system (Omron, Kyoto, Japan). The test tank was constructed with clear acrylic with dimensions of 23 cm in length, 5 cm in width, and 15 cm in depth, and contained 1 L of water. The infrared sensor was positioned 5 cm below the water surface on one side of the test tanks. As the fish passed through the infrared beam, the light reflection was disturbed by the fish and detected by the sensor. Their movements were recorded by a connected computer. Custom software (Scitechkorea Inc., Seoul, Korea) was used to analyze recorded signals and presented as double-plot actograms calculated based on the number of sensor counts per hour. Zebrafish were individually tested in the tank, and their activities were monitored for 72 h.

2.7 | Immunofluorescence Staining

The whole brains of the zebrafish were harvested on ice and immediately fixed in 4% formaldehyde (Samchun, Seoul, Korea) for 2 h at 4°C. Subsequently, the tissues were cryoprotected in 30% sucrose-PBS solution for 16 h at 4°C and then embedded in O.C.T compound (Sakura Finetek, Koto, Japan) on dry ice. The brains were coronally sectioned into 6 μm thick slices using a cryostat (CM3050; Leica, Wetzlar, Germany) and mounted onto coated slides (Matsunami Glass Ind., Ltd., Osaka, Japan). To enhance antigen detection, the heat-induced epitope retrieval method was employed using 10 mM citrate buffer (pH 6.0). The tissues were then blocked with 10% normal goat serum (Jackson ImmunoReseach, West Grove, PA) for 1 h and incubated with primary antibodies specific for *O*-GlcNAc (RL-2), OGT, c-FOS (Santa Cruz, TX, USA), OGA (Proteintech, IL, USA), H2B *O*-GlcNAc (S112), H3(tri methyl K4) (Abcam, Cambridge, UK), ubiquityl-histone H2B (Lys120) (CST, MA, USA), and BDNF (Cusabio, TX, USA). The primary antibody signals were detected using IgG cross-adsorbed Alexa Fluor 488 or 568 secondary antibodies (Invitrogen, CA, USA) and counterstained with DAPI. Images were captured using a confocal LSM 510 META microscope (Carl Zeiss, Jena, Germany) with ×40 magnification and analyzed using ZEN 2009 Light Edition

16000739x, 2024, 5, Downloaded from https://onlinelibrary.wiley.com/doi/10.1111/jpi.13001 by Ewha Womans University Library, Wiley Online Library on [10/11/2024]. See the Terms and Conditions (https://onlinelibrary.wiley.com/terms-and-conditions) on Wiley Online Library for rules of use; OA articles are governed by the applicable Creative Commons License

software. For confocal images, three tissue sections per animal per slide were prepared. Quantification of the images was performed using the ImageJ program.

2.8 | Quantitative Real-Time PCR (qRT-PCR)

Total RNA was extracted using TRIzol (Invitrogen, CA, USA) following the manufacturer's protocols. Complementary DNA (cDNA) was synthesized using GoScript Reverse Transcriptase (Promega, WI, USA) with 1 μg of RNA, the concentration of which was measured using NanoDrop (ND-2000, ThermoFisher Scientific, MA, USA). For qRT-PCR, the cDNA was mixed with Real-Time PCR master mix (BioFact, Daejeon, Korea) and primers and amplified using CFX ConnectTM (BIO-RAD, CA, USA). The cDNAs were amplified with SYBR Green Real-time PCR. The results obtained for each target gene were normalized to β-actin levels using the $\Delta\Delta C_t$ method.

2.9 | Chromatin Immunoprecipitation (ChIP)

To analyze protein-DNA binding, ChIP assays were performed. Cells were fixed in formaldehyde solution (1% formaldehyde, 10 mM NaCl, 5 mM HEPES, pH 7.5, 0.1 mM EDTA, pH 8.0) for 10 min on a rotor at room temperature. After washing with PBS to remove fixation solution, cells were incubated with 125 mM glycine for 5 min on a room temperature rotor. To fragment DNA, samples were sonicated in lysis buffer (0.5% SDS, 5 mM EDTA, 50 mM Tris, pH 8.0, with inhibitors). After the addition of ChIP buffer (0.5% Triton X-100, 2 mM EDTA, 150 mM NaCl, 50 mM Tris, pH 8.0, with inhibitors), the cell lysate was separated by centrifugation. Lysate samples were then incubated overnight at 4°C with primary antibodies specific for H2B *O*-GlcNAc (S112), H3(tri methyl K4) (Abcam), ubiquityl-histone H2B (Lys120) (CST), and OGT (Santa Curz), followed by incubation with protein A agarose (Merck, NJ, USA). After washing the agarose-chromatin complex with ChIP buffer, samples were incubated in elution buffer (1% SDS, 1 mM EDTA, 0.1 M $NaHCO_3$, 50 mM Tris, pH 8.0) for 15 min on a room temperature rotor to separate chromatin from agarose. Following harvest of the supernatant, chromatin was incubated with RNase A (New England Biolabs, MA, USA) and proteinase K (VWR, PA, USA). DNA was precipitated using a mixture of phenol:chloroform:isoamyl alcohol (25:24:1), followed by ethanol precipitation. DNA samples were subsequently analyzed via qRT-PCR with specific primers. The results obtained from ChIP samples for each target were normalized to that of the total sample using the $\Delta\Delta C_t$ method.

2.10 | Primers

The following primers were used for analyzing zebrafish cDNA in this study.: *β-actin* forward, 5′-GTGCCCATCTACG AGGGTTA-3′, *β-actin* reverse, 5′-TCTCAGCTGTGGTGGTGAA G-3′, *bdnf* forward, 5′-GACACTTTCGAGCAGGTCAT-3′, *bdnf* reverse, 5′-GCATACAGGTCAACGTCCTT-3′, *bmal1* forward, 5′-GCTCCACGAGAGAGACTCAT-3′, *bmal1* reverse, 5′- TATTCA GTGGGTTTGACACG-3′, *calm1* forward, 5′-TACATGCATGCA GCTTGAGT-3′, *calm1* reverse, 5′-ATTGAAGCAAACTGCAAA GG-3′, *c-fos* forward, 5′-CTGAGTGTCTCAAGTGCCTC-3′, *c-fos* reverse, 5′-TGGAGGTCTTTGCTCCAGTA-3′, *clock* forward, 5′-ACGATGGGAACATCTCTTGT-3′, *clock* reverse, 5′-CTGCTGTC TCTGGATGTTTG-3′, *cry1a* forward, 5′-GCAAGCCGCCTTAAT ATAGA-3′, *cry1a* reverse, 5′-GATGATGCTGCTGTGTAAGC-3′, *cry1b* forward, 5′-CTGCATTATTGACAGCTTGG-3′, *cry1b* reverse, 5′-CTCTGAAGGAGAAACCTCCA-3′, *nr1d1* forward, 5′-CTGAAAAACATCAGCAGCAC-3′, *nr1d1* reverse, 5′-TAAGG ATGCATGTTCATTGG-3′, *per2* forward, 5′- TGTTTCAGGATGT GGATGAG-3′, *per2* reverse, 5′- AGGAGTCTGTGGATCTGCTC-3′. The following primers were used for analyzing cDNA (mouse) in N2A cell study.: *β-actin* forward, 5′- TCATTGACCTCAACTA CATGGT-3′, *β-actin* reverse, 5′- CTAAGCAGTTGGTGGTGCAG-3′, *bdnf* forward, 5′-CTGACACTTTTGAGCACGTC-3′, *bdnf* reverse, 5′-AACCCATGGGATTACACTTG-3′, *calm1* forward, 5′-GCGACGGACAAGTCAACTAT-3′, *calm1* reverse, 5′-TGCAG ACTTTGTGTGTGGAC-3′, *c-fos* forward, 5′-AACGTGGAGCTG AAGGCAGA-3′, *c-fos* reverse, 5′-AGCTCAGGGAGTCGG AGGAG-3′. The following primers were designed for each promoter site and used to analyze the ChIP results (mouse) in this study.: *bdnf* forward, 5′-AGTGACAGGCGTTGAGAAAG-3′, *bdnf* reverse, 5′-AAGACAAAGCAACTGGCATC-3′, *calm1* forward, 5′-CGTATATATATCGCGGCACAC-3′, *calm1* reverse, 5′-CGCTTCTGC, *c-fos* forward, 5′-CTTGTAGGGTGGTTTTGCAC-3′, *c-fos* reverse, 5′-AAGCAGCAAGTGAAGGATTG-3′.

2.11 | Protein Preparation and Western blot

Total protein was extracted from whole zebrafish brain using ice-cold RIPA buffer (50 mM Tris-pH 7.4, 150 mM NaCl, 0.25% deoxycholic acid, 1% NP-40, 1 mM EDTA-pH 8.0), supplemented with protease, phosphatase, and *O*-GlcNAcase inhibitors (1 mM PMSF, 1 mM DTT, 1 mg/mL aprotinin, 1 mg/mL leupeptin, 1 mM sodium orthovanadate, 1 mM sodium fluoride, 1 mM streptozotocin). To isolate cytosol and nucleus fractions from zebrafish brain, freshly harvested brains (7 brains/group) were homogenized in cytosol extraction buffer (10 mM HEPES, 1.5 mM MgCl2, 200 mM sucrose, 0.5% NP-40, 10 mM KCl) containing protease inhibitors. After 1 h of incubation on ice, the supernatant was separated from the pellet by centrifugation (5000 rpm, 5 min, 4°C). The supernatant was collected as the cytosol sample, and the nucleus protein was extracted from the pellet using nucleus extraction buffer (1 mM EDTA) with sonication. The protein concentration of the extracted samples was determined using a protein assay dye reagent (BIO-RAD). To denature the proteins, ×5 SDS-PAGE sample buffer (Tech & Innovation, Chuncheon, Korea) was added to the samples, which were then boiled at 95°C for 10 min. The protein samples were loaded onto SDS-PAGE gels and separated by electrophoresis using a kit from BIO-RAD. The separated proteins were transferred to a 0.45 μm nitrocellulose membrane (Amersham, Buckinghamshire, UK). After blocking with 5% skim milk (BD Biosciences, NJ, USA) or BSA (RDT, Gyeonggido, Korea) for 1 h at room temperature, the membranes were incubated overnight at 4°C with primary antibodies specific for *O*-GlcNAc (RL-2), OGT, c-FOS, H2B (Santa Cruz), OGA,

16000736, 2024, 5, Downloaded from https://onlinelibrary.wiley.com/doi/10.1111/jpi.13001 by Ewha Womans University Library, Wiley Online Library on [10/11/2024]. See the Terms and Conditions (https://onlinelibrary.wiley.com/terms-and-conditions) on Wiley Online Library for rules of use; OA articles are governed by the applicable Creative Commons License

α-tubulin (Proteintech), H2B *O*-GlcNAc (S112), H3(tri methiyl K4) (Abcam), and BDNF (Cusabio) in blocking solution. After washing, horseradish peroxidase (HRP)-conjugated secondary IgG antibodies were incubated for 1 h at room temperature. The HRP signals were detected using the Enhanced Chemiluminescence (ECL) detection system (Amersham) and visualized using a chemi-doc machine (Universal Hood II; BIO-RAD).

2.12 | Statistical Analysis

All graphs were generated and statistically analyzed using Prism software (version 8; GraphPad, CA, USA). Results are presented as means ± standard error of the mean (SEM). To determine significant differences between two groups, the Mann-Whitney test was employed. For comparisons among more than two groups, the Kruskal-Wallis test with the original false discovery rate (FDR) correction method of Benjamini and Hochberg was applied. A two-way ANOVA was conducted for behavioral data analysis, with Tukey's multiple comparisons test to assess differences between groups. For within-group comparisons, the Friedman test with ANOVA was performed. Statistical significance was defined as $p < 0.05$.

3 | Results

3.1 | Light-Dark Phase Inversion Disrupts Circadian Rhythm and Impairs Memory Function in Adult Zebrafish

To establish a circadian disruption model, adult zebrafish were subjected to an altered light-dark cycle compared to the control group under a normal light-dark cycle (LD). Specifically, the group subjected to disruption experienced inversion of the light-dark phase, where the dark period was initiated from 8 a.m. to 8 p.m. and light period from 8 p.m. to 8 a.m. (DL) for 3 consecutive days in a dark box (Figure 1A). Behavioral pattern analysis confirmed alterations in the circadian rhythm. The actogram test revealed changes in sleep-wake patterns, whereby control fish exhibited predominantly diurnal activity while DL fish showed decreased daytime and increased nighttime activity on the first day of circadian disruption (Figure 1B). However, activity patterns in DL fish returned to control levels from day 2 of the light-dark inversion induction (Figure 1B). Although DL fish exhibited nearly similar activity patterns as the control group on Day 3, analysis of circadian rhythm gene expression levels in zebrafish brain disclosed significant differences. In the control group, rhythmic expression patterns of *nr1d1*, *bmal1*, *cry1a*, and *clock* genes were observed (Figure 1C). Notably, DL zebrafish exhibited opposite rhythmic expression patterns of the above genes as the control group. Furthermore, the expression pattern of *cry1b* in DL was opposite that of the control group, although rhythmic variations of this gene within each group were not significant (Figure 1C). No marked expression changes were observed for *per2* in either the control or DL group. Subsequently, the fear conditioning (FC) test was conducted to assess the impact of circadian rhythm disruption on learning and memory (L/M) ability (Supporting Information S1: Figure 1). The control group demonstrated prolonged crossing times during learning trials, which persisted into the memory session (Figure 1D). L/M performance declined slightly in the group subjected to DL for 1 day but was significantly impaired in zebrafish exposed to DL for 3 days, highlighting the detrimental effect of prolonged circadian rhythm disruption on cognitive ability.

3.2 | Circadian Disruption Dysregulates Rhythmic Circadian Expression of *O*-GlcNAc Cycling

Previous research highlights the importance of the *O*-GlcNAc/HBP cycle in L/M ability in hippocampus of the brain. Here, we investigated the circadian rhythmic patterns of *O*-GlcNAc cycling in zebrafish brain. To this end, *O*-GlcNAc levels were evaluated via immunofluorescence staining within the hippocampal region at 4 h intervals beginning at 8 a.m. We observed a gradual elevation in *O*-GlcNAc levels, peaking at 8 p.m. followed by a decline, with this peak being delayed and attenuated after 3 days of light-dark exposure. In the dark-light group, basal levels of *O*-GlcNAc were maintained during the dark phase (8 a.m. to 8 p.m.) but increased and peaked at 4 a.m. during the light phase (Figure 2A). To further clarify the relationship between *O*-GlcNAc changes and circadian rhythm, the levels of OGT and OGA were assessed. Strong correlations were observed between the daily expression patterns of OGT and *O*-GlcNAcylation oscillation (Figure 2B). OGA exhibited distinct oscillation patterns, increasing after OGT and *O*-GlcNAc peak times and decreasing before light re-exposure (Figure 2C). However, DL induction resulted in diminished OGA expression throughout the day. Western blot quantification of the levels of *O*-GlcNAcylation, OGT, and OGA in whole-brain homogenates revealed no apparent differences across various time points (Supporting Information S1: Figure 2). Subsequent analysis of cytosolic and nuclear proteins disclosed a rhythmic pattern of *O*-GlcNAc and OGT expression in nuclear fractions, with peak levels observed at 0 a.m. Both OGT and *O*-GlcNAc levels in the nuclear fractions were decreased in the DL group of zebrafish (Figure 2D). Additionally, cytosolic OGA levels increased from 8 p.m. to 4 a.m., which was diminished in the DL group (Figure 2D). However, attempts to detect OGA in the nuclear fraction were unsuccessful. These findings highlight the intricate interplay between *O*-GlcNAc cycling and circadian rhythm regulation in zebrafish brain.

3.3 | Treatment With Melatonin During the Light Phase Alters the Rhythmic Patterns of *O*-GlcNAc Cycling

We further analyzed the impact of melatonin, a well-known hormone involved in the regulation of circadian rhythms, on *O*-GlcNAc cycling. Initially, effects were evaluated at the cellular level. Treatment of N2A cells with various concentrations of melatonin (0, 1, 5, 10, 50, 100 μM) for 24 h resulted in a significant decrease in *O*-GlcNAc and OGT levels, which were particularly notable at a concentration of 100 μM, whereas OGA levels remained unchanged (Figure 3A). Subsequently, exposure to 100 μM melatonin at different time points (0, 0.5, 2, 6,

16000793x, 2024, 5, Downloaded from https://onlinelibrary.wiley.com/doi/10.1111/jpi.13001 by Ewha Womans University Library, Wiley Online Library on [10/11/2024]. See the Terms and Conditions (https://onlinelibrary.wiley.com/terms-and-conditions) on Wiley Online Library for rules of use; OA articles are governed by the applicable Creative Commons License

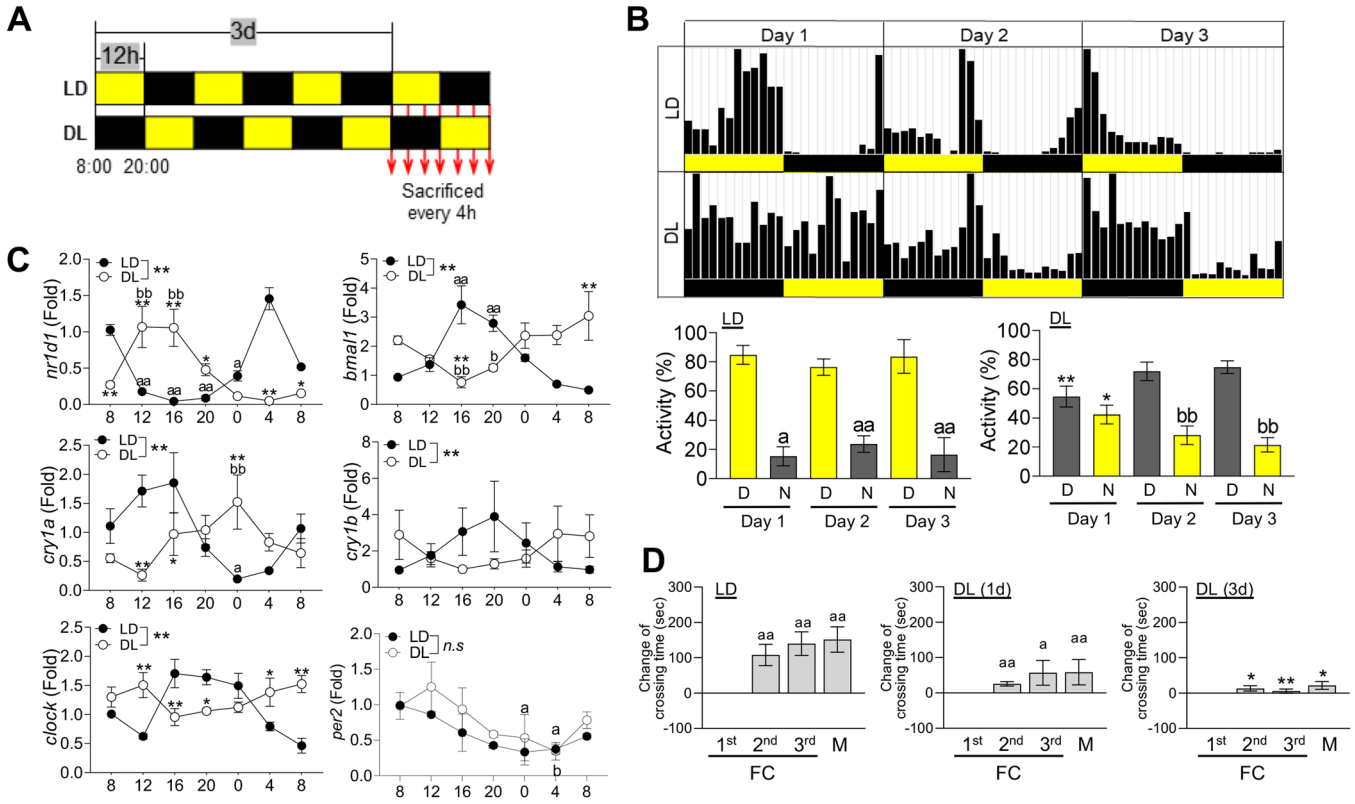


FIGURE 1 | Light-dark cycle inversion-induced circadian disruption in adult zebrafish. To establish a circadian disruption adult zebrafish model, the light-dark phase was reversed. The lighting conditions were automatically controlled within the light-dark box. Under LD conditions, zebrafish were exposed to 12 h of light daily from 8 a.m. to 8 p.m., while under DL conditions, light exposure was reversed from 8 p.m. until 8 a.m. the following day. (A) Schematic representation of the experimental plan. Yellow and black indicate the light exposure and dark period, respectively. (B) Representative summary actograms depicting zebrafish activity under LD and DL conditions over 3 days. Bars represent activity counts per hour, and the graph shows activity percentage per day over the 3-day period. Statistical analyses involved within-group comparisons using the Friedman ANOVA test with the original Benjamini and Hochberg false discovery rate (FDR) ($^{a}p < 0.05$, $^{aa}p < 0.01$ vs. each time-point of LD; $^{bb}p < 0.01$ vs. each time-point of DL). Between-group comparisons were conducted using two-way ANOVA with Tukey's multiple comparison test ($*p < 0.05$, $**p < 0.01$ vs. Con). (C) After 3 days of exposure to DL, zebrafish were killed, and brain samples were collected every 4 h over the next 24 h. mRNA expression in zebrafish brain ($n = 4$/group) was measured via quantitative real-time PCR with the appropriate primers. Bars represent the mean ± SEM of target gene expression normalized to β-actin levels using the $\Delta\Delta C_t$ method. Statistical analysis involved within-group comparisons using two-way ANOVA with the original Benjamini and Hochberg FDR ($^{a}p < 0.05$, $^{aa}p < 0.01$ vs. 8 a.m. of LD; $^{b}p < 0.05$, $^{bb}p < 0.01$ vs. 8 a.m. of DL). Between-group comparisons were conducted using two-way ANOVA with Tukey's multiple comparisons test ($*p < 0.05$, $**p < 0.01$ vs. LD). (D) Graphs illustrating changes in crossing times compared to the first learning session after 1 or 3 days of circadian disruption. Crossing times were measured for up to 5 min during three learning sessions (FC) and one memory session (M), conducted 2 h after the final learning session. Error bars represent the mean ± SEM ($n = 7$–12/group). Within-group comparisons were performed using two-way ANOVA with the original Benjamini and Hochberg FDR ($^{a}p < 0.05$, $^{aa}p < 0.01$ vs. 1st learning). Between-group comparisons were conducted using two-way ANOVA with Tukey's multiple comparisons test ($*p < 0.05$, $**p < 0.01$ vs. LD).

12, and 24 h) led to a decrease in *O*-GlcNAc and OGT levels at 24 h after initiation of treatment. Consistently, no alterations in OGA levels were observed in response to melatonin (Figure 3B). In keeping with protein expression patterns, *ogt* mRNA levels showed a decrease at 24 h in the presence of 100 μM melatonin (Supporting Information S1: Figure 3). Unexpectedly, melatonin exerted a suppressive effect on *oga* mRNA expression despite no impact on the protein level.

Next, we investigated whether melatonin influences rhythmic *O*-GlcNAc/HBP cycling in zebrafish brain. To this end, melatonin was intraperitoneally injected into zebrafish for three consecutive days at 8 a.m. immediately after the onset of the light phase (Mel, Figure 3C). Analysis of zebrafish activity patterns revealed disrupted normal daytime activity for 2 days, which returned to normal on Day 3 (Figure 3D). Notably, rhythmic circadian clock gene expression remained largely unchanged following melatonin administration during the light phase (Figure 3E). Interestingly, while melatonin treatment during the light phase impaired zebrafish L/M function after 3 days, no such effect was observed when melatonin was administered at the onset of the dark phase (8 p.m.) (Figure 3F). In terms of rhythmic *O*-GlcNAc cycling in zebrafish brain, exposure to melatonin during the light phase failed to induce the expected increase in levels of *O*-GlcNAc, OGT, and OGA at 8 p.m. compared to 8 a.m. In contrast, melatonin treatment during the dark phase resulted in elevation of *O*-GlcNAc levels at 8 p.m. compared to 8 a.m. (Figure 3G; Supporting Information S1: Figure 4A).

16000781x, 2024, 5, Downloaded from https://onlinelibrary.wiley.com/doi/10.1111/jpi.13001 by Ewha Womans University Library, Wiley Online Library on [10/11/2024]. See the Terms and Conditions (https://onlinelibrary.wiley.com/terms-and-conditions) on Wiley Online Library for rules of use; OA articles are governed by the applicable Creative Commons License

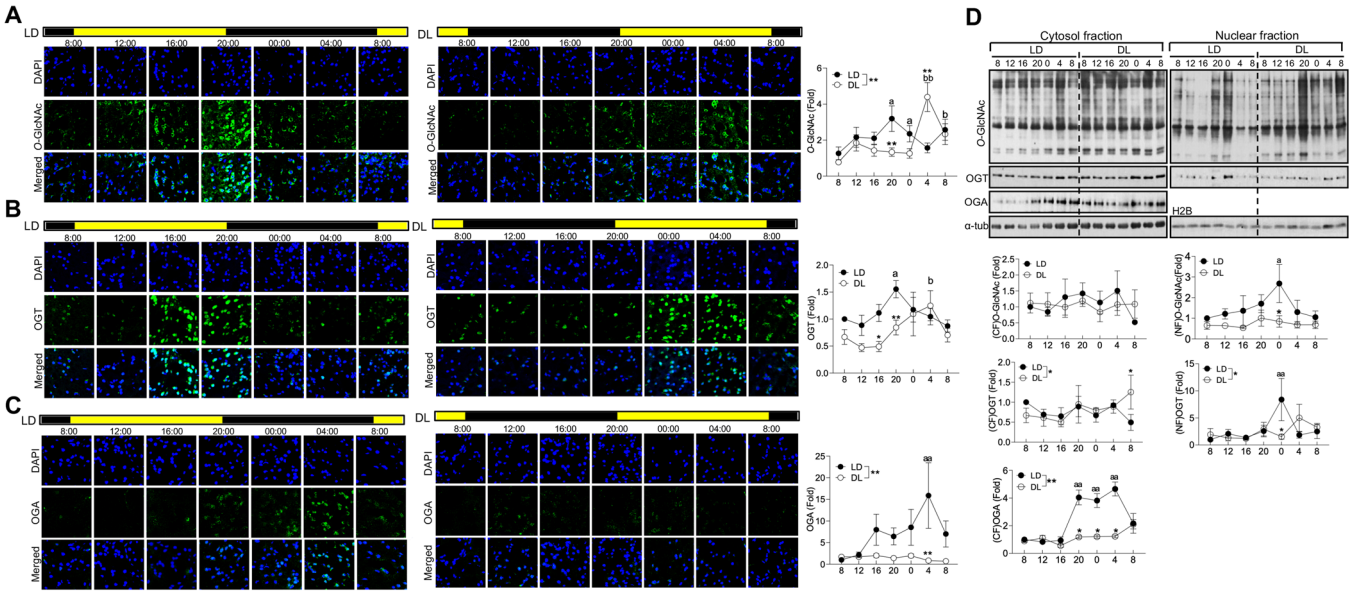


FIGURE 2 | Circadian regulation of *O*-GlcNAc cycling. After 3 days of LD or DL induction, zebrafish were killed and brain samples harvested every 4 h for analysis. (A–C) Representative confocal images (×40 magnification) showing DAPI (blue), *O*-GlcNAc (A, green), OGT (B, green), OGA (C, green), and merged immunofluorescence staining in the dorsal lateral (Dl) region of the telencephalon area in zebrafish brain. The graphs display quantitative results for each antibody, normalized to DAPI levels ($n = 3$–4/group). Statistical analysis included within-group comparisons using the two-way ANOVA test with the original Benjamini and Hochberg FDR ($^{a}p < 0.05$, $^{aa}p < 0.01$ vs. 8 a.m. of LD, $^{b}p < 0.05$, $^{bb}p < 0.01$ vs. 8 p.m. of DL). Between-group comparisons were conducted using two-way ANOVA with Tukey's multiple comparisons test ($^{*}p < 0.05$, $^{**}p < 0.01$ vs. LD). (D) To separate cytosolic (CE) and nuclear (NE) proteins, a pool of zebrafish whole brain extracts (7 brains/group) was used. Protein samples were normalized to total protein content before denaturation and analyzed via western blot. Bars represent the mean ± SEM of target protein expression normalized to α-tubulin (CE) or H2B (NE) levels. For statistical analysis, within-group comparisons were conducted using the two-way ANOVA test with the original Benjamini and Hochberg FDR ($^{a}p < 0.05$, $^{aa}p < 0.01$ vs. 8 a.m. of LD). Between-group comparisons were performed using two-way ANOVA with Tukey's multiple comparisons test ($^{*}p < 0.05$, $^{**}p < 0.01$ vs. LD).

3.4 | Circadian Expression Patterns of Genes Regulating Neuronal Function Are Disrupted by Circadian Phase Inversion and Light-Phase Melatonin Treatment

Numerous factors regulate learning and memory, including neurotransmitters, receptors, neurotrophic factors, and synaptic proteins. Among these, we investigated the rhythmic expression patterns of *c-fos, bdnf, and calm1* in zebrafish brain under normal LD compared with DL conditions or light-phase melatonin treatment. In control zebrafish brain, *calm1* was significantly decreased at the onset of the dark phase (8 p.m.) relative to onset of the light phase (8 a.m.) while both *c-fos and bdnf* showed no significant changes (Figure 4A,B). However, the DL and the light phase melatonin-treated groups exhibited differential expression patterns of *c-fos, bdnf, and calm1* relative to the normal DL group. Interestingly, protein levels of c-Fos and BDNF in the LD group displayed rhythmic expression, peaking at 8 p.m. and 12 p.m., respectively. These rhythmic changes were abolished in both the DL and light phase melatonin-treated group (Figure 4C,D).

3.5 | Circadian Regulation of Histone H2B *O*-GlcNAcylation and H3K4 Methylation in Zebrafish Brain is Disrupted Under Circadian Phase Inversion and Light-Phase Melatonin Treatment Conditions

Genes involved in the regulation of brain function, such as *c-fos*, *bdnf*, and *calm1*, are transcriptionally modulated through epigenetic changes, in particular, H3K4me3 [37, 38]. Additionally, H3K4me3 regulation is linked with Ser112 *O*-GlcNAcylation of histone 2B (H2B *O*-Glc) mediated by OGT in the nucleus [27, 39]. Using immunofluorescence staining, we observed circadian changes in H2B *O*-Glc, which began to increase continuously from 8 p.m. until 4 a.m. and returned to basal levels by 8 a.m. (Figure 5A,C). However, under DL conditions, a distinct expression pattern was observed, with a peak at 12 a.m. followed by a decrease, while the light-phase melatonin treatment group showed an overall significant decrease in H2B *O*-Glc. Importantly, dark-phase melatonin treatment induced a normal increase in H2B *O*-Glc and c-Fos at 8 p.m. similar to the control group (Supporting Information S1: Figure 4B,C). In the control LD group, the circadian rhythmic expression of H3K4me3 was similar to that of H2B *O*-Glc, while in both the DL and light-phase melatonin treatment groups, overall H3K4me3 expression was significantly reduced (Figure 5B,D). Data from an earlier study suggest that *O*-GlcNAcylation and ubiquitination in histone 2B can reciprocally regulate one another [27]. However, in our experiments, that H2B ubiquitination (H2B Ub) was not significantly changed over the course of the light phase and remained unaffected under DL (Supporting Information S1: Figure 5).

3.6 | An OGT Inhibitor, OSMI-1, Disrupts the Circadian Cycle and L/M Function in Zebrafish

The impacts of the OGT inhibitor, OSMI-1, on the circadian rhythm and brain function of zebrafish were further examined. Intracranial injection of OSMI-1 for three consecutive days resulted in disruption of circadian regulation of *O*-GlcNAcylation

16000793x, 2024, 5, Downloaded from https://onlinelibrary.wiley.com/doi/10.1111/jpi.13001 by Ewha Womans University Library, Wiley Online Library on [10/11/2024]. See the Terms and Conditions (https://onlinelibrary.wiley.com/terms-and-conditions) on Wiley Online Library for rules of use; OA articles are governed by the applicable Creative Commons License

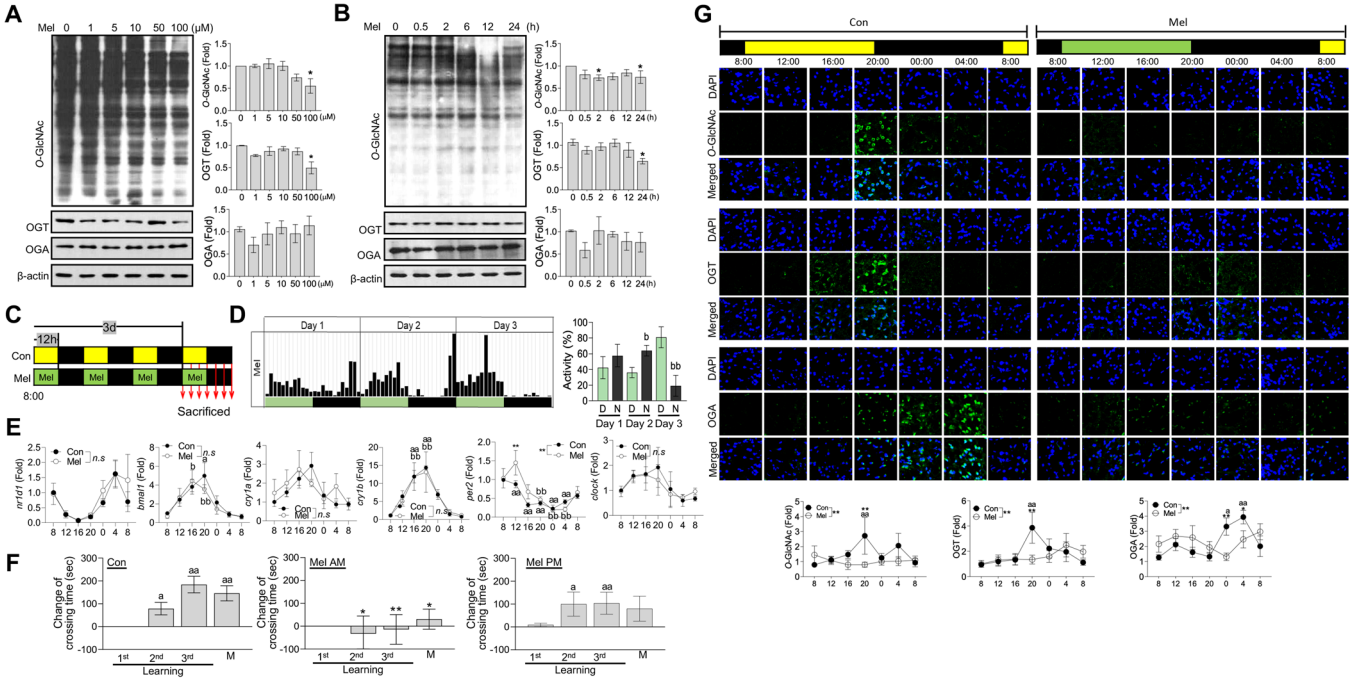


FIGURE 3 | Melatonin-induced changes in *O*-GlcNAc cycling. (A) N2A cells were treated with the indicated doses of melatonin and harvested at 24 h. Total protein levels were assessed via western blot assay with specific antibodies. The graphs represent the quantities of *O*-GlcNAc, OGT, and OGA normalized to β-actin levels. Experiments were independently replicated three times. For statistical analysis, the Mann-Whitney test was performed ($^{*}p < 0.05$ vs. 0 μM). (B) N2A cells were treated with 100 μM melatonin for the indicated times and harvested. The graphs represent the quantities of *O*-GlcNAc, OGT, and OGA normalized to β-actin levels. The experiments were independently replicated three times. For statistical analysis, the Mann-Whitney test was performed ($^{*}p < 0.05$ vs. 0 h). (C) Schematic illustration of the experimental plan. All fish were exposed to 12 h of light daily from 8 a.m. to 8 p.m. In the melatonin treatment group (Mel), melatonin was intraperitoneally injected at 8 a.m. once a day for 3 days and brains harvested every 4 h for subsequent experiments. Yellow and black indicate the light exposure and dark times, respectively. (D) Representative summary actograms of the melatonin treatment group for 3 days. Bars represent activity counts per hour. For statistical analysis, within-group comparison was conducted using the Friedman ANOVA test with the original Benjamini and FDR ($^{b}p < 0.05$, $^{bb}p < 0.01$ vs. Mel). (E) mRNA expression levels of zebrafish brains ($n = 3$/group) were measured via quantitative real-time PCR using the appropriate primers. Bars represent the mean ± SEM of target gene expression normalized to β-actin levels using the $\Delta\Delta C_t$ method. For statistical analysis, within-group comparison was conducted using the two-way ANOVA test with the original Benjamini and Hochberg FDR ($^{a}p < 0.05$, $^{aa}p < 0.01$ vs. 8 a.m. of Con, $^{b}p < 0.05$, $^{bb}p < 0.01$ vs. 8 a.m. of Mel). Between-group comparisons were performed using two-way ANOVA with Tukey's multiple comparisons test (n.s). (F) Graphs representing the changes in crossing times compared to those during the first learning session. After 1 or 3 days of circadian disruption, crossing times were measured for up to 5 min in three learning sessions (FC) and one memory session (M). The memory session was conducted 2 h after the final learning session. Error bars represent the mean ± SEM ($n = 7$–12/group). For statistical analysis, within-group comparison was conducted using the two-way ANOVA test with the original Benjamini and Hochberg FDR ($^{aa}p < 0.01$ vs. 1st learning). Between-group comparisons were performed using two-way ANOVA with Tukey's multiple comparisons test ($^{*}p < 0.05$, $^{**}p < 0.01$ vs. Con). (G) Representative confocal images (×40 magnification) of DAPI (blue), *O*-GlcNAc (upper, green), OGT (middle, green), OGA (bottom, green), and merged immunofluorescence staining of the Dl region of the telencephalon area in zebrafish brain are shown. The graphs display quantitative results for each antibody with normalization based on DAPI levels ($n = 3$/group). For statistical analysis, within-group comparison was conducted using the two-way ANOVA test with the original Benjamini and Hochberg FDR ($^{a}p < 0.05$, $^{aa}p < 0.01$ vs. 8 a.m. of Con). Between-group comparisons were performed using two-way ANOVA with Tukey's multiple comparisons test ($^{*}p < 0.05$, $^{**}p < 0.01$ Mel).

and histone H2B *O*-GlcNAcylation (Figure 6A). Interestingly, while OSMI-1 did not significantly alter the rhythmic expression of circadian clock genes, normal sleep-wake activity patterns of the fish were impaired (Figure 6B,C). Furthermore, circadian expression of c-FOS and BDNF was significantly decreased at both mRNA and protein levels (Figure 6D,E), and L/M function of zebrafish was impaired by OSMI-1 (Figure 6F).

3.7 | OSMI-1 Disrupts Circadian *O*-GlcNAc Cycling in N2A Cells

N2A cells were treated with OSMI-1, and changes in *O*-GlcNAc oscillation over a 24 h period examined at 4 h intervals. Rhythmic regulation of *O*-GlcNAcylation, which peaked at 12 h in the control group, was abolished by OSMI-1 treatment. Interestingly, OSMI-1 induced an increase in OGT expression from 12 h onwards, which persisted until 24 h, in N2A cells (Figure 7A). The increased expression of c-Fos, starting at 16 h in control cells, was not observed in OSMI-1-treated cells. Next, binding of OGT and histone modifications (H2B *O*-Glc, H3K4me3, and H2B Ub) at the promoter sites of *c-fos, bdnf*, and *calm1* were analyzed in control N2A cells for comparison with OSMI-1-treated cells. OSMI-1 significantly reduced binding of H2B *O*-Glc and OGT at the promoter sites relative to untreated controls (Figure 7B). H3K4me3 binding was increased at the *c-fos* promoter but decreased at the *bdnf* promoter, while binding of H2B Ub to promoters of *c-fos, bdnf*, and *calm1* was not affected by OSMI-1.

16000730x, 2024, 5, Downloaded from https://onlinelibrary.wiley.com/doi/10.1111/jpi.13001 by Ewha Womans University Library, Wiley Online Library on [10/11/2024]. See the Terms and Conditions (https://onlinelibrary.wiley.com/terms-and-conditions) on Wiley Online Library for rules of use; OA articles are governed by the applicable Creative Commons License

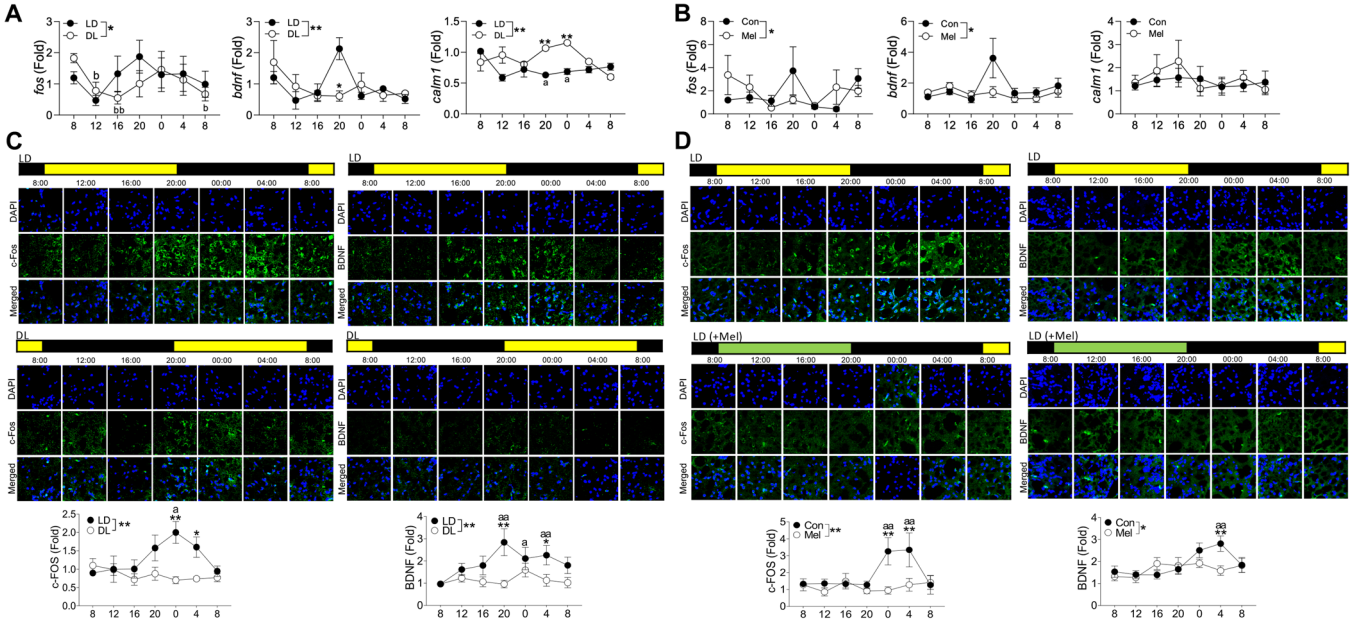


FIGURE 4 | Circadian regulation of c-Fos, BDNF, and Calm1 in the zebrafish brain. Light-dark phase inversion (DL) or light-phase melatonin treatment (Mel) was applied for 3 days. (A, B) mRNA expression levels in zebrafish brains ($n = 3$/group) were measured via quantitative real-time PCR every 4 h with the appropriate primers. Bars represent the mean ± SEM of target gene expression normalized to β-actin levels using the $\Delta\Delta C_t$ method. For statistical analysis, within-group comparison was conducted using the Friedman ANOVA test with the original Benjamini and Hochberg FDR ($^{a}p < 0.05$, $^{aa}p < 0.01$ vs. 8 a.m. of Con, $^{bb}p < 0.01$ vs. 8 a.m. of Mel). Between-group comparisons were performed using two-way ANOVA with Tukey's multiple comparisons test ($^{*}p < 0.05$, $^{**}p < 0.01$ vs. LD). (C, D) Representative confocal images (at ×40 magnification) of DAPI (blue), c-FOS or BDNF (green), and merged immunofluorescence staining of the dorsal lateral (Dl) region of the telencephalon area in zebrafish brain are shown. Graphs display quantitative results for each antibody with normalization based on DAPI levels ($n = 3$/group). For statistical analysis, within-group comparison was conducted using the Friedman ANOVA test with the original Benjamini and Hochberg FDR ($^{a}p < 0.05$, $^{aa}p < 0.01$ vs. 8 a.m. of Con). Between-group comparisons were performed using two-way ANOVA with Tukey's multiple comparisons test ($^{*}p < 0.05$, $^{**}p < 0.01$ vs. DL or Mel).

Consistently, mRNA levels of *c-fos, bdnf*, and *calm1* were suppressed by OSMI-1 in N2A cells (Figure 7C).

4 | Discussion

Light serves as the primary signal for animals to synchronize their circadian clocks with the day/night cycle, which is crucial for coordinating physiological and behavioral processes with environmental changes. Central to this mechanism is the ability of light to initiate changes in gene expression. Despite its importance, our understanding of the precise molecular mechanisms underlying light-induced gene expression remains incomplete. Zebrafish offers an effective model for investigating circadian rhythms in view of its responsiveness to direct light exposure and induction of clock gene expression across various tissues that facilitate the adjustment of intrinsic clocks within the organism. In the current study, inverting the light-dark (LD) to dark-light (DL) cycle over 3 days resulted in circadian cycle disruption, as evident from alterations in activity and expression patterns of circadian genes. Intriguingly, DL induced dysfunction of fear-context memory, consistent with previous findings, further highlighting the negative effects of disturbed sleep and night shift work on cognitive function. The role of the circadian clock in cognition, particularly memory formation and consolidation, is currently an active focus of research. While the circadian control of sleep is one of the mechanisms implicated in memory regulation, growing evidence also suggests a direct involvement of the circadian clock in memory processes independent of sleep regulation.

Recent findings from our zebrafish and mouse models consistently demonstrate that sleep deprivation disrupts the HBP glucose metabolism pathway in the brain, with effects on *O*-GlcNAc cycling and impairment of memory function [36, 40, 41]. This study was conducted under the assumption that circadian disruption disrupts *O*-GlcNAc cycling in brain, leading to defects in normal brain function. While 24 h rhythmic oscillation of cellular protein *O*-GlcNAcylation has been observed in peripheral systems in response to clock-controlled feeding-fasting cycles in *Drosophila* [42], its rhythmic oscillation in the central nervous system in response to the light-dark cycle has not been explored to date. We have conclusively demonstrated that *O*-GlcNAcylation of proteins in the brain exhibits daily rhythmic oscillations throughout the light-dark cycle independent of the feeding cycle. Furthermore, the rhythmic oscillation of OGT and OGA enzymes expression patterns is associated with this daily cycling of *O*-GlcNAc. The collective findings represent the first step toward elucidating the pivotal role of light-specific circadian regulation in orchestrating *O*-GlcNAc cycling within the brain.

In this study, we employed two zebrafish circadian disruption models to examine alterations in the daily rhythm of *O*-GlcNAcylation and underlying mechanisms of resulting brain functional abnormalities. In one model, circadian disruption was induced by inverting the light-dark cycle over 3 days, while in the other, circadian disruption was triggered by daytime administration of melatonin secreted from the pineal gland under dark external conditions for 3 days. Interestingly,

16000739x, 2024, 5, Downloaded from https://onlinelibrary.wiley.com/doi/10.1111/jpi.13001 by Ewha Womans University Library, Wiley Online Library on [10/11/2024]. See the Terms and Conditions (https://onlinelibrary.wiley.com/terms-and-conditions) on Wiley Online Library for rules of use; OA articles are governed by the applicable Creative Commons License

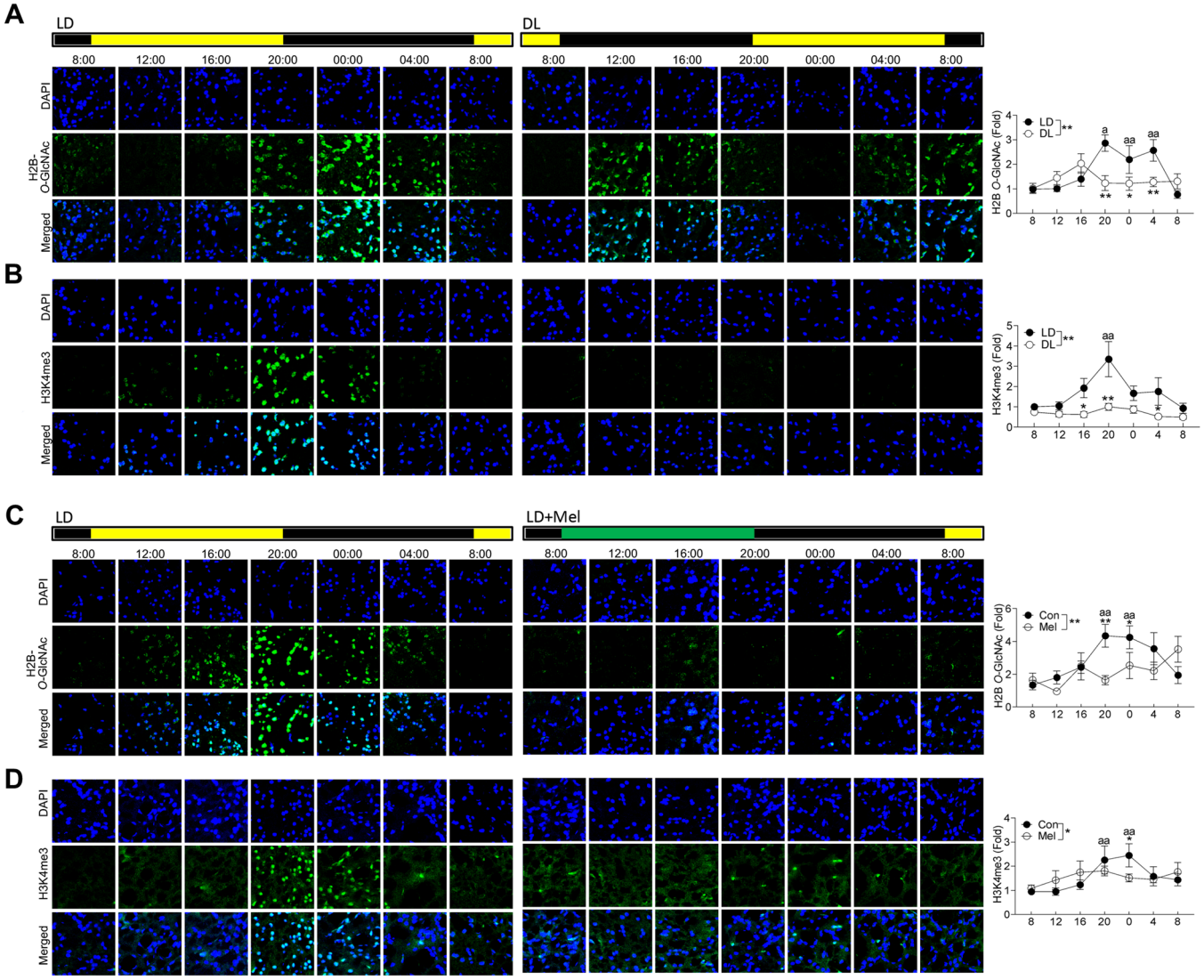


FIGURE 5 | Circadian regulation of histone H2B *O*-GlcNAcylation and H3K4 methylation. Zebrafish were exposed to light-dark phase inversion (DL) or light-phase melatonin treatment (Mel) for 3 days, followed by harvesting of brain samples every 4 h and immunofluorescence staining using specific antibodies. Representative confocal images (×40 magnification) of DAPI (blue), H2B *O*-GlcNAc (A, C: green), H3K4me3 (B, D: green), and merged immunofluorescence staining regions of the Dl region of the telencephalon area in zebrafish brain are shown. Graphs display quantitative results for each antibody with normalization based on DAPI levels ($n = 3$/group). For statistical analysis, within-group comparison was conducted using the two-way ANOVA test with the original Benjamini and Hochberg FDR ($^{aa}p < 0.01$ vs. 8 a.m. of Con). Between-group comparisons were performed using two-way ANOVA with Tukey's multiple comparisons test ($^{*}p < 0.05$, $^{**}p < 0.01$ vs. DL or Mel).

both models elicited numerous common molecular, physiological, and functional changes in the brain while also displaying distinct patterns and regulatory functions. The disruption of circadian gene oscillation in the LD inverting model was evident, with the exception of *per2*. Despite *per2* being a well-known light-driven gene, its expression remained unchanged. This discrepancy may be attributed to differences between mRNA and protein levels. Circadian genes are regulated not only at the transcriptional level but also through processes such as protein translation and posttranslational modifications. Remarkably, both DL and melatonin models induced cognitive impairment and suppression of molecules involved in synaptic plasticity regulation, such as c-Fos, BDNF, and Calm1. Additionally, disruption of the normal rhythmic cycling of *O*-GlcNAcylation and expression of OGT and OGA were observed in both models. Intriguingly, melatonin treatment during the dark phase did not affect *O*-GlcNAc cycling, c-Fos levels, or L/M ability. The two circadian disruption models also exhibited distinct features. Specifically, while circadian disruption induced by the light-dark cycle shift resulted in a switch in the rhythmic patterns of *O*-GlcNAcylation and OGT between day and night, circadian disruption induced by melatonin administration led to an overall reduction in the levels of *O*-GlcNAcylation, OGT, and OGA in the brain. Despite nuanced differences in regulatory mechanisms between the models, the overarching implication that circadian disruption disrupts the rhythmicity of *O*-GlcNAc cycling, potentially contributing to functional impairments in the brain, remains consistent.

Our data confirmed daily rhythmicity of histone H2B *O*-GlcNAcylation and H3K4 trimethylation (H3K4me3), which was significantly disrupted or attenuated in both the light-dark

16000793x, 2024, 5, Downloaded from https://onlinelibrary.wiley.com/doi/10.1111/jpi.13001 by Ewha Womans University Library, Wiley Online Library on [10/11/2024]. See the Terms and Conditions (https://onlinelibrary.wiley.com/terms-and-conditions) on Wiley Online Library for rules of use; OA articles are governed by the applicable Creative Commons License

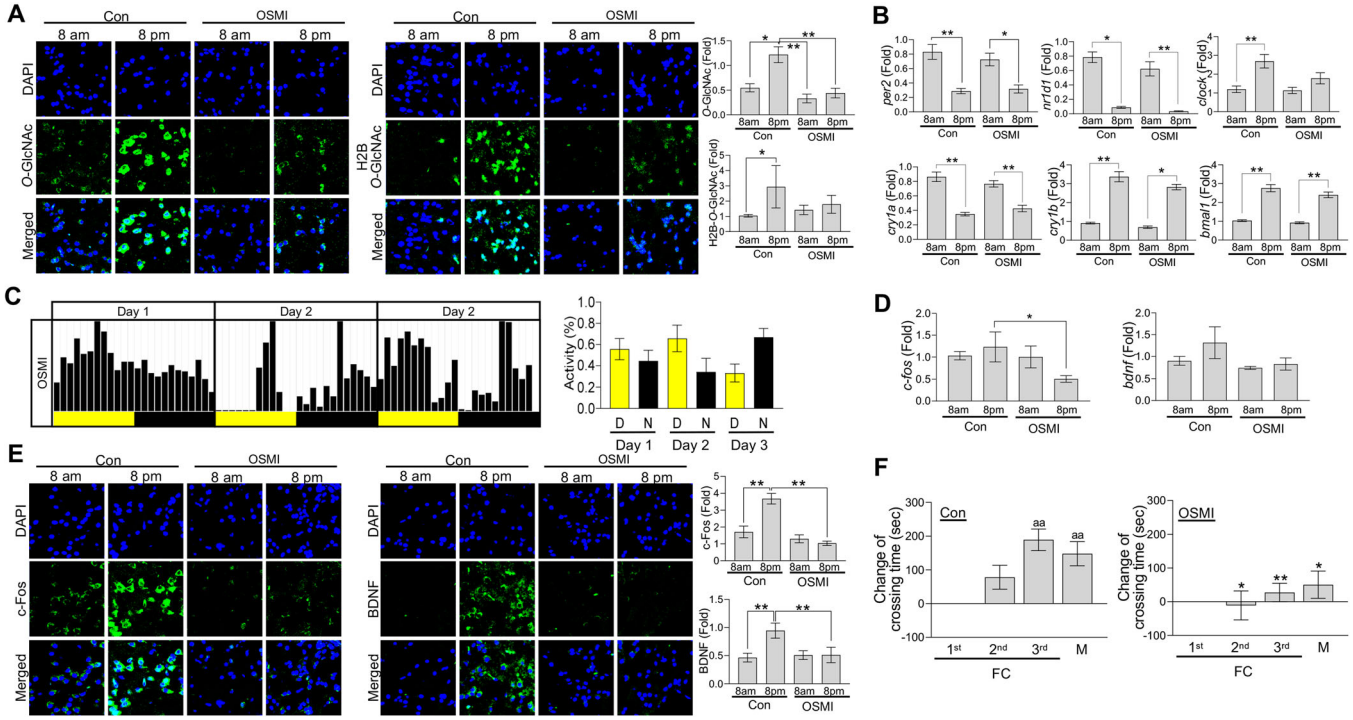


FIGURE 6 | Circadian regulation of zebrafish by OGT inhibitor, OSMI-1. All fish were exposed to 12 h of light daily from 8 a.m. to 8 p.m. In the treatment group, OSMI (0.01 ng/g) was intracranially injected at 8 p.m. once a day for three consecutive days. Brains were harvested at 8 a.m. and 8 p.m. for analysis. (A) Representative confocal images (×40) of the telencephalon area Dl region in zebrafish brain showing DAPI staining (blue), *O*-GlcNAc (left, green), H2B *O*-GlcNAc (right, green), and merged immunofluorescence. Quantitative results of immunofluorescence were normalized based on DAPI levels ($n = 3$/group). Quantitative results of immunofluorescence are displayed with normalization based on DAPI levels ($n = 3$/group). Statistical analysis was performed using Friedman ANOVA test with the Benjamini and Hochberg false discovery rate (FDR) method (*$p < 0.05$, **$p < 0.01$). (B) Quantitative real-time PCR analysis of mRNA expression levels in zebrafish brains ($n = 3$/group), normalized to β-actin levels using the $\Delta\Delta C_t$ method. Statistical analysis was conducted using Friedman ANOVA test with the Benjamini and Hochberg FDR method (*$p < 0.05$, **$p < 0.01$). (C) The bars represent activity counts per hour and the graph displays activity percentage per day for 3 days. Within-group comparison utilized Friedman ANOVA test with the Benjamini and Hochberg FDR (n.s), while between-group comparisons were performed using two-way ANOVA with Tukey's multiple comparisons test (n.s). (D) Quantitative real-time PCR analysis of mRNA levels in zebrafish brain ($n = 3$/group) normalized to that of β-actin using the $\Delta\Delta C_t$ method. Statistical analysis was conducted using Friedman ANOVA test with the Benjamini and Hochberg FDR method (*$p < 0.05$, **$p < 0.01$). (E) Representative confocal images (×40) of zebrafish brain Dl region showing DAPI staining (blue), c-FOS (left, green), BDNF (right, green), and merged immunofluorescence. Quantitative results with normalization based on DAPI levels are presented ($n = 3$/group). Statistical analysis was performed using Friedman ANOVA test with the Benjamini and Hochberg FDR method (*$p < 0.05$, **$p < 0.01$). (F) Fear-conditioned learning and memory tests. Changes in crossing times compared to the first learning session were measured for up to 5 min in three learning sessions and one memory session (M). Error bars represent mean ± SEM ($n = 9$–11/group). Within-group comparison utilized Friedman ANOVA test with the Benjamini and Hochberg FDR ($^{aa}p < 0.01$ vs. 1st learning), while between-group comparisons were performed using two-way ANOVA with Tukey's multiple comparisons test (*$p < 0.05$, **$p < 0.01$ vs. Con).

inversion and melatonin-treated circadian disruption models. Based on these findings, we hypothesized that rhythmicity of *O*-GlcNAc cycling regulates the histone code, potentially influencing the periodic expression of various genes, including circadian genes and neurotransmitters. While the pattern of H3K4me3 oscillation is similar to that of H2B *O*-GlcNAcylation, chromatin immunoprecipitation (ChIP) results suggest that H2B *O*-Glc increases binding to the promoters of *c-fos*, *bdnf*, and *calm1* independently of H3K4me3 or H2B ubiquitination. Previous research indicates that OGT associates with the TET family to regulate H3K4me3 [30]. Additionally, OGT is reported to form a complex with Mixed Lineage Leukemia 5 (MLL5) and Ubiquitin Specific Protease 7 (USP7) that acts to regulate the stability of MLL5 [43]. These results suggest that OGT is involved in gene expression, not only through H2B *O*-GlcNAcylation but also by independently regulating histone methylation and ubiquitination. Therefore, the rhythmic expression patterns of OGT and *O*-GlcNAcylation are speculated to be part of the intricate mechanisms regulating gene expression, which require further exploration via Chip-seq analysis.

In summary, this study focuses on the significance of comprehending the molecular mechanisms underlying circadian disruption and its effects on brain function. Our data offer valuable insights into potential therapeutic targets for alleviating cognitive impairments linked to disruption of circadian rhythms. Continued exploration of the regulatory mechanisms governing circadian rhythm-induced *O*-GlcNAc cycling and histone modifications is crucial for fully understanding their involvement in brain function and cognitive processes.

16000739x, 2024, 5, Downloaded from https://onlinelibrary.wiley.com/doi/10.1111/jpi.13001 by Ewha Womans University Library, Wiley Online Library on [10/11/2024]. See the Terms and Conditions (https://onlinelibrary.wiley.com/terms-and-conditions) on Wiley Online Library for rules of use; OA articles are governed by the applicable Creative Commons License

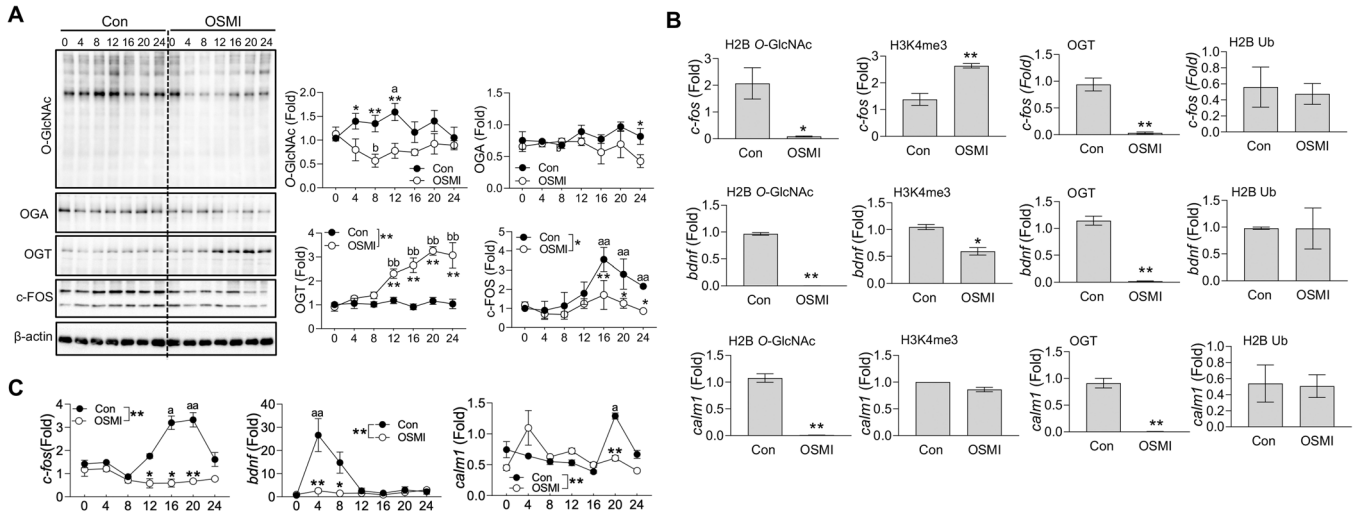


FIGURE 7 | OSMI-1-induced inhibition of OGT and H2B-*O*-GlcNAc binding to promoter sites of neuronal plasticity genes in N2A cells. For circadian rhythm synchronization, N2A cells were treated for 90 min with 200 nM dexamethasone in DMEM containing 0.25% FBS. The medium was replaced with fresh DMEM containing 0.25% FBS supplemented with OSMI-1 (50 μM) or 0.1% DMSO. (A) Protein expression levels of *O*-GlcNAcylation, OGT, OGA, and c-Fos were analyzed by harvesting N2A cells every 4 h up to 24 h after OSMI-1 treatment, followed by western blot with specific primary antibodies. The bars represent the mean ± SEM of target protein expression normalized to α-tubulin levels. Statistical analysis for within-group comparison was conducted using the two-way ANOVA test with the original Benjamini and Hochberg FDR ($^{a}p < 0.05$, $^{aa}p < 0.01$ vs. 0 h). A two-way ANOVA with Tukey's multiple comparisons test was performed for between-group comparisons ($^{*}p < 0.05$, $^{**}p < 0.01$ vs. Con). (B) mRNA expression levels were analyzed by harvesting N2A cells every 4 h up to 24 h after OSMI treatment, followed by quantitative real-time PCR with specific primers. The bars represent the mean ± SEM of target gene expression normalized to β-actin levels using the $\Delta\Delta C_t$ method. Statistical analysis for within-group comparison was conducted using the two-way ANOVA test with the original Benjamini and Hochberg FDR ($^{a}p < 0.05$, $^{aa}p < 0.01$ vs. 0 h). A two-way ANOVA with Tukey's multiple comparisons test was performed for between-group comparisons ($^{*}p < 0.05$, $^{**}p < 0.01$ vs. Con). (C) Protein-DNA binding at the promoter regions of brain function-related genes was analyzed in cells at 12 h after OSMI treatment via ChIP assays. ChIP-DNA was analyzed via real-time qPCR at the indicated promoter regions. The unpaired *t*-test was performed for comparisons between two groups ($^{*}p < 0.05$, $^{**}p < 0.01$ vs. Con).

Author Contributions

Jiwon Park and Dong Yeol Kim designed and conducted the experiments, analyzed the data, prepared the figures, and wrote the main manuscript text. Eok-Soo Oh analyzed the data and contributed to revising the manuscript. Inn-Oc Han Han designed the experiments, analyzed the data, and wrote the main manuscript. All authors reviewed the manuscript.

Acknowledgments

This work was supported by National Research Foundation (NRF) of Korea Grants (RS-2024-00346770) and Research Grant of Inha University.

Ethics Statement

All studies were procedure in accordance with the guidelines of the Institutional Animal Care and Use Committee of the Inha University in Incheon (INHA 220719-832).

Conflicts of Interest

The authors declare no conflicts of interest.

Data Availability Statement

The data and materials used in this research are available upon request from the corresponding author.

References

1. M. Menaker, "Circadian Clocks: 50 Years on," *Cold Spring Harbor Symposia on Quantitative Biology* 72 (2007): 655–659.

2. A. Patke, M. W. Young, and S. Axelrod, "Molecular Mechanisms and Physiological Importance of Circadian Rhythms," *Nature Reviews Molecular Cell Biology* 21 (2020): 67–84.

3. Y. Li and I. P. Androulakis, "Light Entrainment of the SCN Circadian Clock and Implications for Personalized Alterations of Corticosterone Rhythms in Shift Work and Jet Lag," *Scientific Reports* 11 (2021): 17929.

4. Z. Ben-Moshe, N. S. Foulkes, and Y. Gothilf, "Functional Development of the Circadian Clock in the Zebrafish Pineal Gland," *BioMed Research International* 2014 (2014): 1–8.

5. T. K. Tamai, L. C. Young, and D. Whitmore, "Light Signaling to the Zebrafish Circadian Clock by Cryptochrome 1a," *Proceedings of the National Academy of Sciences of the United States of America* 104 (2007): 14712–14717.

6. J. Mendoza, "Circadian Clocks: Setting Time by Food," *Journal of Neuroendocrinology* 19 (2007): 127–137.

7. A. R. Neves, T. Albuquerque, T. Quintela, and D. Costa, "Circadian Rhythm and Disease: Relationship, New Insights, and Future Perspectives," *Journal of Cellular Physiology* 237 (2022): 3239–3256.

8. X. Pan, S. Mota, and B. Zhang, "Circadian Clock Regulation on Lipid Metabolism and Metabolic Diseases," *Advances in Experimental Medicine and Biology* 1276 (2020): 53–66.

9. I. Aiello, M. L. M. Fedele, F. Román, et al., "Circadian Disruption Promotes Tumor-Immune Microenvironment Remodeling Favoring Tumor Cell Proliferation," *Science Advances* 6 (2020): eaaz4530.

16000793x, 2024, 5, Downloaded from https://onlinelibrary.wiley.com/doi/10.1111/jpi.13001 by Ewha Womans University Library, Wiley Online Library on [10/11/2024]. See the Terms and Conditions (https://onlinelibrary.wiley.com/terms-and-conditions) on Wiley Online Library for rules of use; OA articles are governed by the applicable Creative Commons License

10. Y. Leng, E. S. Musiek, K. Hu, F. P. Cappuccio, and K. Yaffe, "Association Between Circadian Rhythms and Neurodegenerative Diseases," *Lancet Neurology* 18 (2019): 307–318.

11. A. V. Goltsev, E. A. P. Wright, J. F. F. Mendes, and S. Yoon, "Generation and Disruption of Circadian Rhythms in the Suprachiasmatic Nucleus: A Core-Shell Model," *Journal of Biological Rhythms* 37 (2022): 545–561.

12. H. Jamshed, R. Beyl, D. Della Manna, E. Yang, E. Ravussin, and C. Peterson, "Early Time-Restricted Feeding Improves 24-Hour Glucose Levels and Affects Markers of the Circadian Clock, Aging, and Autophagy in Humans," *Nutrients* 11 (2019): 1234.

13. M. L. Dubocovich, R. L. Hudson, I. C. Sumaya, M. I. Masana, and E. Manna, "Effect of MT1 Melatonin Receptor Deletion on Melatonin-Mediated Phase Shift of Circadian Rhythms in the C57BL/6 Mouse," *Journal of Pineal Research* 39 (2005): 113–120.

14. C. A. Czeisler, R. E. Kronauer, J. S. Allan, et al., "Bright Light Induction of Strong (Type 0) Resetting of the Human Circadian Pacemaker," *Science* 244 (1989): 1328–1333.

15. S. Yamazaki, R. Numano, M. Abe, et al., "Resetting Central and Peripheral Circadian Oscillators in Transgenic Rats," *Science* 288 (2000): 682–685.

16. F. O. James, N. Cermakian, and D. B. Boivin, "Circadian Rhythms of Melatonin, Cortisol, and Clock Gene Expression During Simulated Night Shift Work," *Sleep* 30 (2007): 1427–1436.

17. J. Bass, "Circadian Topology of Metabolism," *Nature* 491 (2012): 348–356.

18. S. Panda, "Circadian Physiology of Metabolism," *Science* 354 (2016): 1008–1015.

19. G. W. Hart, "Nutrient Regulation of Signaling and Transcription," *Journal of Biological Chemistry* 294 (2019): 2211–2231.

20. D. J. Durgan, B. M. Pat, B. Laczy, et al., "O-GlcNAcylation, Novel Post-Translational Modification Linking Myocardial Metabolism and Cardiomyocyte Circadian Clock," *Journal of Biological Chemistry* 286 (2011): 44606–44619.

21. K. Kaasik, S. Kivimäe, J. J. Allen, et al., "Glucose Sensor O-GlcNAcylation Coordinates With Phosphorylation to Regulate Circadian Clock," *Cell Metabolism* 17 (2013): 291–302.

22. M. D. Li, H. B. Ruan, M. E. Hughes, et al., "O-GlcNAc Signaling Entrains the Circadian Clock by Inhibiting BMAL1/CLOCK Ubiquitination," *Cell Metabolism* 17 (2013): 303–310.

23. K. Xu, J. R. DiAngelo, M. E. Hughes, J. B. Hogenesch, and A. Sehgal, "The Circadian Clock Interacts With Metabolic Physiology to Influence Reproductive Fitness," *Cell Metabolism* 13 (2011): 639–654.

24. B. D. Strahl and C. D. Allis, "The Language of Covalent Histone Modifications," *Nature* 403 (2000): 41–45.

25. T. Kouzarides, "Chromatin Modifications and Their Function," *Cell* 128 (2007): 693–705.

26. H. He, "Global Effects of Histone Modifications," *Briefings in Functional Genomics and Proteomics* 2 (2003): 234–243.

27. R. Fujiki, W. Hashiba, H. Sekine, et al., "GlcNAcylation of Histone H2B Facilitates Its Monoubiquitination," *Nature* 480 (2011): 557–560.

28. R. Pavri, B. Zhu, G. Li, et al., "Histone H2B Monoubiquitination Functions Cooperatively with FACT to Regulate Elongation By RNA Polymerase II," *Cell* 125 (2006): 703–717.

29. K. Sakabe and G. W. Hart, "O-GlcNAc Transferase Regulates Mitotic Chromatin Dynamics," *Journal of Biological Chemistry* 285 (2010): 34460–34468.

30. R. Deplus, B. Delatte, M. K. Schwinn, et al., "TET2 and TET3 Regulate GlcNAcylation and H3K4 Methylation Through OGT and SET1/COMPASS," *The EMBO Journal* 32 (2013): 645–655.

31. M. Iida, Y. Nakane, T. Yoshimura, and T. Hirota, "Effects of Cryptochrome-Modulating Compounds on Circadian Behavioural Rhythms in Zebrafish," *Journal of Biochemistry* 171 (2022): 501–507.

32. G. Oikonomou, M. Altermatt, R. Zhang, et al., "The Serotonergic Raphe Promote Sleep in Zebrafish and Mice," *Neuron* 103 (2019): 686–701.e8.

33. M. C. Beker, B. Caglayan, A. B. Caglayan, et al., "Interaction of Melatonin and Bmal1 in the Regulation of PI3K/AKT Pathway Components and Cellular Survival," *Scientific Reports* 9 (2019): 19082.

34. S. Narishige, M. Kuwahara, A. Shinozaki, et al., "Effects of Caffeine on Circadian Phase, Amplitude and Period Evaluated in Cells in Vitro and Peripheral Organs in Vivo in PER2::LUCIFERASE Mice," *British Journal of Pharmacology* 171 (2014): 5858–5869.

35. M. Malcolm, L. Saad, L. G. Penazzi, and E. Garbarino-Pico, "Processing Bodies Oscillate in Neuro 2A Cells," *Frontiers in Cellular Neuroscience* 13 (2019): 487.

36. J. Park, D. Y. Kim, G. S. Hwang, and I. O. Han, "Repeated Sleep Deprivation Decreases the Flux into Hexosamine Biosynthetic Pathway/O-GlcNAc Cycling and Aggravates Alzheimer's Disease Neuropathology in Adult Zebrafish," *Journal of Neuroinflammation* 20 (2023): 257.

37. J. Y. Joo, K. Schaukowitch, L. Farbiak, G. Kilaru, and T. K. Kim, "Stimulus-Specific Combinatorial Functionality of Neuronal c-fos Enhancers," *Nature Neuroscience* 19 (2016): 75–83.

38. T. H. Beacon, G. P. Delcuve, C. López, et al., "The Dynamic Broad Epigenetic (H3K4me3, H3K27ac) Domain as a Mark of Essential Genes," *Clinical Epigenetics* 13 (2021): 138.

39. S. Zhang, K. Roche, H. P. Nasheuer, and N. F. Lowndes, "Modification of Histones by Sugar β-N-acetylglucosamine (GlcNAc) Occurs on Multiple Residues, Including Histone H3 Serine 10, and is Cell Cycle-Regulated," *Journal of Biological Chemistry* 286 (2011): 37483–37495.

40. S. M. Kim, S. Zhang, J. Park, et al., "REM Sleep Deprivation Impairs Learning and Memory by Decreasing Brain O-GlcNAc Cycling in Mouse," *Neurotherapeutics* 18 (2021): 2504–2517.

41. Y. Lee, J. Park, S. M. Kim, et al., "Sleep Deprivation Impairs Learning and Memory by Decreasing Protein O-GlcNAcylation in the Brain of Adult Zebrafish," *FASEB Journal* 34 (2020): 853–864.

42. X. Liu, I. Blaženović, A. J. Contreras, et al., "Hexosamine Biosynthetic Pathway and O-GlcNAc-Processing Enzymes Regulate Daily Rhythms in Protein O-GlcNAcylation," *Nature Communications* 12 (2021): 4173.

43. X. Ding, W. Jiang, P. Zhou, et al., "Mixed Lineage Leukemia 5 (MLL5) Protein Stability Is Cooperatively Regulated By O-GlcNAc Transferase (OGT) and Ubiquitin Specific Protease 7 (USP7)," *PLoS One* 10 (2015): e0145023.

Supporting Information

Additional supporting information can be found online in the Supporting Information section.

16000739x, 2024, 5, Downloaded from https://onlinelibrary.wiley.com/doi/10.1111/jpi.13001 by Ewha Womans University Library, Wiley Online Library on [10/11/2024]. See the Terms and Conditions (https://onlinelibrary.wiley.com/terms-and-conditions) on Wiley Online Library for rules of use; OA articles are governed by the applicable Creative Commons License